Charge transfer of N^{4+} with atomic hydrogen

B. Zygelman
Department of Physics, University of Nevada, Las Vegas, Las Vegas, Nevada 89154

D. L. Cooper and M. J. Ford
Department of Chemistry, University of Liverpool, P. O. Box 147, Liverpool L69 3BX, United Kingdom

A. Dalgarno
Harvard Smithsonian Center for Astrophysics, 60 Garden Street, Cambridge, Massachusetts 02138

J. Gerratt
School of Chemistry, University of Bristol, Cantocks Close, Bristol BS8 1TS, United Kingdom

M. Raimondi
Dipartimento di Chimica Fisica ed Elettrochimica, Universitá di Milano, Via Golgi 19, 20133 Milano, Italy
(Received 10 February 1992)

State-dependent cross sections and rate coefficients for the charge-transfer process $N^{4+}+H\rightarrow N^{3+}(2s3l)+H^{+}$ for $l=s,p,d$ in the collision-energy range from 0.1 eV to 8 keV are presented. A close-coupled quantum-mechanical method is employed, and it is argued that the molecular-state expansion method without translation factors is a valid low-energy approximation for charge-transfer processes. We show that the method does not suffer from the electron-origin problem. The spin-coupled valence-bond method is used to construct both *ab initio* potential curves and adiabatic coupling elements. The calculated cross sections exhibit variations with energy, which we propose are a manifestation of Stueckelberg oscillations. The cross sections are compared with measured total cross sections for electron capture by N^{4+} ions in collisions with hydrogen. Agreement is excellent in the collision-energy range from 4.1 to 182 eV/amu.

PACS number(s): 34.70.+e

I. INTRODUCTION

Charge transfer of multiply charged ions is important in determining the ionization distribution in laboratory and astrophysical plasmas produced by near thermal ionizing sources, and the resulting emission lines are valuable diagnostic probes of the neutral components of the plasma.

Theoretical investigations of the state-dependent direct charge-transfer processes

$$N^{4+}(2s)+H\rightarrow N^{3+}(3s3l)+H^{+} \quad (1)$$

for $l=s,p,d$ were undertaken by Feickert *et al.* [1] using a coupled-channel quantum-mechanical method. They obtained cross sections and rate coefficients (1) for gas temperatures in the range between 30 to 10^5 K. Cross sections for the total charge-transfer process

$$N^{4+}+H\rightarrow N^{3+}+H^{+} \quad (2)$$

were measured by Huq, Havener, and Phaneuf [2] using a merged-beam apparatus for collision energies from 1.2 to 982 eV/amu.

In this study we calculate the cross sections and rate coefficients for the process (1) in the center-of-mass collision-energy range from 0.1 eV to 8 keV using a fully quantum-mechanical method. We improve the calculation of Ref. [1] by performing a full *ab initio* calculation of the potential curves and coupling elements for states of the NH^{4+} molecular ion. We insure that the potentials tend at large distances to the polarization form so that the low-energy behavior of the cross sections is correctly predicted. The spin-coupled valence-bond (SCVB) method is used to calculate adiabatic coupling elements. The adiabatic potentials and the coupling elements are then used to construct diabatic potential curves and diabatic coupling elements. At low energies, rotational coupling to the Π states may be ignored and we restrict the investigation to charge transfer involving the singlet $^1\Sigma$ states of the NH^{4+} ion. In Sec. III we review the scattering theory used in the present calculation. The results and discussion are presented in Sec. IV. Unless otherwise stated, atomic units are used throughout.

II. SCVB CALCULATIONS

The spin-coupled valence-bond or SCVB approach to electronic structure is a powerful *ab initio* technique that provides accurate, compact descriptions of ground- and excited-state potential-energy surfaces. The single-configuration spin-coupled approach has been applied to a very wide range of chemical problems and has provided important insight into the structure and bonding in whole series of molecular systems. Multiconfiguration SCVB calculations have concentrated mostly on diatomic and triatomic species. Previous studies of charge-transfer systems and multiply charged ions include, among many others, the CH^{3+} and CLi^{3+} systems [3] and the H_2O^{2+}

cation [4]. A number of reviews of the SCVB approach are available [5], including a detailed survey of representative recent applications [6].

The spin-coupled wave function for an N-electron system is based on a single spatial configuration with one singly occupied orbital for each electron. In general, the N orbitals $\phi_1,\phi_2,\ldots,\phi_N$ are all distinct and nonorthogonal. The spin-coupled wave function consists of an antisymmetrized product of this single spatial configuration and a linear combination of the complete set of N-electron spin functions $\{\Theta^N_{SM;k} k=1,2,\ldots,f^N_S\}$ corresponding to total spin S (and projection M). The spin-coupled wave function is thus an eigenfunction of both $\hat{S}^2$ and $\hat{S}_Z$. For a four-electron system with no net spin ($S=0$), the dimension of the spin space is $f^N_S=2$.

The spin-coupled wave function for NH^{4+} takes the form

$$\Psi_{SM}=\sum_{k=1}^{f^N_S} c_{Sk}(N!)^{1/2}A(\phi_1\phi_2\phi_3\phi_4\Theta^N_{SM;k}) , \tag{3}$$

in which A is the antisymmetrizing operator and the c_{Sk}, which reflect the relative importance of the different modes of spin coupling, may be termed spin-coupling coefficients. Each of the orbitals was expanded in a basis set $\{\chi_p\}$,

$$\phi_\mu=\sum_{p=1}^{m} c_{\mu p}\chi_p , \tag{4}$$

without any restrictions on the form of the orbitals or on the overlaps between them. The basis set used in the present work for N-H consists of $(12s7p3d/5s2p1d)$ Gaussian-type orbitals (GTO's) contracted to $[6s4p3d/3s2p1d]$. Spherical GTO's were used (5 d components), resulting in a total of 47 basis functions. This basis set, which is listed in Table I, is of triple-ζ-valence quality, augmented with diffuse functions and polarization functions. The $c_{\mu p}$ in Eq. (4) and the c_{Sk} in Eq. (3) were fully optimized simultaneously by means of a powerful procedure that utilizes the second derivatives of the energy with respect to the variational parameters. Further details of the computational techniques are available in the review articles cited above.

For all geometries considered, the converged spin-coupled orbitals for the lowest singlet state of NH^{4+} were found to possess pure σ symmetry and could be characterized as

$$\phi_1\approx N^{3+}(1s),\quad \phi_2\approx N^{3+}(1s') ,$$
$$\phi_3\approx N^{3+}(2s),\quad \phi_4\approx N^{3+}(2s') .$$

At convergence, each of the spin-coupled orbitals satisfies an equation that can be cast in the form

$$\hat{F}^{\text{eff}}_\mu\phi_\mu=\varepsilon_\mu\phi_\mu , \tag{5}$$

where the Hermitian operators $\hat{F}^{\text{eff}}_\mu(\mu=1,2,\ldots N)$ are constructed from $N-1$ electron quantities in which occupied orbital ϕ_μ is missing. Each operator generates a complete set or stack of orthonormal solutions, which we denote $\phi^{(i)}_\mu$ $(i=1,2,\ldots,m)$. The orbitals $\phi^{(i)}_\mu$ correspond to the motion of one electron in the field of the other $N-1$ electrons. In general, orbitals in different stacks are not orthogonal to one another. One solution in each stack, usually $\phi^{(1)}_\mu$, coincides with the occupied orbital ϕ_μ. The remaining orbitals are termed virtual orbitals and provide excellent first approximations to excited states.

TABLE I. Exponents α and contraction coefficients k_i for the GTO basis set used in the SCVB calculations.

	Nitrogen			Hydrogen	
Type	k_1	α_i	Type	k_i	α_i
s	0.000 760	13520.	s	0.025 374	33.64
	0.006 076	1999.		0.189 684	5.058
	0.032 847	440.0		0.852 933	1.147
	0.132 396	120.9	s	1.0	0.3211
	0.393 261	38.47	s	1.0	0.1013
	0.546 339	13.46	p	1.0	1.0
s	0.252 036	13.46	p	1.0	0.3
	0.779 385	4.993	d	1.0	0.3
s	1.0	1.5690			
s	1.0	0.5800			
s	1.0	0.1923			
s	1.0	0.05			
p	0.016 916	35.91			
	0.102 200	8.480			
	0.338 134	2.706			
	0.669 281	0.9921			
p	1.0	0.3727			
p	1.0	0.1346			
p	1.0	0.06			
d	1.0	1.8			
d	1.0	0.6			
d	1.0	0.2			

Wave functions for excited states, as well as an improved description of the ground state, may be obtained by means of a nonorthogonal configuration-interaction calculation involving the spin-coupled configuration and typically 10^2-10^3 excited configurations. These excited configurations are generated by replacing one, two, or more occupied orbitals by virtual orbitals from their respective stacks. Such replacements are termed vertical excitations. The final multiconfiguration wave functions, known as spin-coupled valence-bond or SCVB wave functions, take the form

$$\Psi_{SM}=\sum_{i_1\cdots i_N}\sum_k c_{Sk}(i_1\cdots i_N)(N!)^{1/2} \times A(\phi_1^{(i_1)}\phi_2^{(i_2)}\cdots\phi_N^{(i_N)}\Theta^N_{SM;k}) . \tag{6}$$

Each spatial configuration may generate more than one valence-bond (VB) structure, on account of the different modes of spin coupling labeled by the index k. The coefficients $c_{Sk}(i_1\ldots i_N)$ for each state, and the corresponding total energies, are determined by constructing the matrix of the Hamiltonian and the overlap matrix over the chosen set of structures, and solving the usual secular problem.

Excited spin-coupled configurations for NH^{4+} were generated by means of single and double replacements of

orbitals ϕ_3 and ϕ_4 by virtual orbitals taken from their own stacks. In addition to these vertical excitations, configurations were included in which one orbital is doubly occupied. The chosen set of virtual orbitals consists of $5\sigma, 3\pi, 1\delta$ virtuals from stack 3 and of $6\sigma, 3\pi, 1\delta$ virtuals from stack 4. This gives rise to a total of 135 spatial configurations (241 VB structures) of $^1\Sigma^+$ symmetry.

The eight lowest roots were extracted from the SCVB calculations; the calculated total energies are reported in Table II. Asymptotic energies for these eight states are compared with experimental data in Table III. The SCVB values were obtained by removing the Coulombic repulsion in the $N^{3+}+H^+$ states from the corresponding SCVB energies for a nuclear separation of 30 bohr. These eight states span a range of more than 60 eV. The asymptotes relevant to the charge-transfer process are $N^{4+}(2s)+H(1s)$ and the three $N^{3+}(2s3l)+H^+$ channels. It is clear from Table III that these asymptotic splittings are reproduced fairly well. The main limitation of the current SCVB calculations is the quality of the modest GTO basis set rather than the need to include further virtual orbitals and excited configurations. Asymptotically, the $N^{4+}(2s)+H$ potential behaves as $-32/R^4$, close to the exact value $-36/R^4$.

Matrix elements of $\partial/\partial R$ were calculated from these compact SCVB wave functions by numerical differentiation. This required separate SCVB calculations for nuclear separations of $R-\delta$ and $R+\delta$ in order to generate wave functions $\Psi_i(\mathbf{r}/R-\delta)$ and $\Phi_i(\mathbf{r}|R+\delta)$, where the index i labels the different states. The overlap integrals between GTO's calculated for the nuclear separation R were then used to form the quantity

$$\frac{\langle \Psi_i(\mathbf{r}|R-\delta)|\Psi_j(\mathbf{r}|R+\delta)\rangle}{2\delta} . \tag{7}$$

This simple central difference approximation to $\langle \Psi_i|\partial/\partial R|\Psi_j\rangle$ does not take full account of the changes in the basis functions with R. Calculations that included this term also suggest that its contribution is small, at least for NH^{4+}, but that its inclusion can make this procedure numerically unstable and very sensitive to the choice of δ. One criterion for the consistency of the numerical differentiation employed here is the equality

$$\left\langle \Psi_i \left| \frac{\partial}{\partial R} \right| \Psi_j \right\rangle = -\left\langle \Psi_j \left| \frac{\partial}{\partial R} \right| \Psi_i \right\rangle , \tag{8}$$

which is typically satisfied to at least four significant figures. The values of $\langle \Psi_i|\partial/\partial R|\Psi_j\rangle$ obtained by means of Eq. (7) are not very sensitive to the value of δ and, indeed, the optimum value of δ remains constant over a

TABLE II. Potential-energy curves (adiabatic) from SCVB calculations for the eight lowest $^1\Sigma^+$ states of NH^{4+}.

R (bohr)	Energy (hartree)							
	(1)	(2)	(3)	(4)	(5)	(6)	(7)	(8)
2.00	−49.758 436	−49.244 874	−48.823 818	−48.538 674	−48.206 061	−47.838 140	−47.785 531	-47.666 169
3.00	−50.191 980	−49.607 899	−49.309 605	−49.060 428	−48.772 188	−48.382 073	−48.309 475	−48.197 111
3.50	−50.327 942	−49.731 397	−49.447 343	−49.204 263	−48.858 200	−48.472 863	−48.463 826	−48.357 601
3.75	−50.383 281	−49.783 215	−49.503 137	−49.262 041	−48.881 990	−48.531 890	−48.497 557	−48.421 375
4.00	−50.432 023	−49.829 514	−49.552 142	−49.312 788	−48.897 886	−48.588 196	−48.527 604	−48.470 781
4.25	−50.475 245	−49.870 911	−49.595 502	−49.357 726	−48.908 315	−48.638 350	−48.567 358	−48.499 308
4.50	−50.513 824	−49.908 037	−49.634 160	−49.397 795	−48.915 180	−48.682 937	−48.611 729	−48.515 979
4.75	−50.548 455	−49.941 495	−49.668 813	−49.433 700	−48.919 838	−48.722 367	−48.653 732	−48.552 024
5.00	−50.579 702	−49.971 786	−49.700 042	−49.466 045	−48.923 350	−48.756 930	−48.691 443	−48.589 630
5.25	−50.608 030	−49.999 304	−49.728 348	−49.495 423	−48.926 660	−48.786 893	−48.724 627	−48.622 835
5.50	−50.633 756	−50.024 555	−49.754 240	−49.522 755	−48.930 700	−48.812 349	−48.753 020	−48.652 099
5.75	−50.657 359	−50.047 614	−49.777 984	−49.546 827	−48.935 530	−48.834 055	−48.777 794	−48.678 489
6.00	−50.679 031	−50.068 968	−49.799 593	−49.569 716	−48.942 276	−48.852 337	−48.798 222	−48.702 282
6.25	−50.699 013	−50.088 571	−49.819 233	−49.591 400	−48.951 359	−48.868 261	−48.813 854	−48.723 017
6.50	−50.717 422	−50.106 648	−49.837 841	−49.610 664	−48.961 951	−48.882 899	−48.825 304	−48.742 687
6.75	−50.734 472	−50.123 434	−49.855 018	−49.628 237	−48.973 529	−48.897 075	−48.832 724	−48.760 557
7.00	−50.750 312	−50.139 057	−49.870 915	−49.644 409	−48.985 509	−48.910 956	−48.837 143	−48.776 834
7.25	−50.765 062	−50.153 623	−49.885 640	−49.659 275	−48.997 469	−48.924 423	−48.839 623	−48.791 684
7.50	−50.778 664	−50.167 227	−49.898 627	−49.668 971	−49.009 082	−48.937 425	−48.841 022	−48.804 834
7.75	−50.791 697	−50.179 953	−49.912 485	−49.686 001	−49.020 460	−48.949 846	−48.841 748	−48.817 129
8.00	−50.803 766	−50.191 884	−49.924 561	−49.698 184	−49.031 253	−48.961 527	−48.842 716	−48.827 876
8.25	−50.815 095	−50.203 155	−49.935 829	−49.709 332	−49.041 544	−48.972 577	−48.847 040	−48.833 929
8.50	−50.825 778	−50.213 854	−49.946 459	−49.720 432	−49.051 364	−48.983 031	−48.855 517	−48.835 030
8.75	−50.835 838	−50.223 950	−49.957 088	−49.730 275	−49.060 665	−48.993 012	−48.864 824	−48.834 550
9.00	−50.845 352	−50.233 634	−49.966 475	−49.739 551	−49.069 553	−49.002 366	−48.873 971	−48.834 028
9.50	−50.862 881	−50.251 299	−49.983 926	−49.757 189	−49.086 070	−49.019 667	−48.891 170	−48.832 655
10.00	−50.878 684	−50.267 094	−49.999 791	−49.773 685	−49.101 101	−49.035 267	−48.906 838	−48.831 497
15.00	−50.978 513	−50.366 786	−50.099 034	−49.871 038	−49.198 366	−49.134 199	−49.005 873	−48.828 497
20.00	−51.028 500	−50.416 690	−50.148 944	−49.921 039	−49.247 942	−49.183 824	−49.055 645	−48.828 120
30.00	−51.078 496	−50.466 644	−50.198 895	−49.971 039	−49.297 787	−49.233 599	−49.105 511	−48.827 960

TABLE III. Asymptotic energies (in eV) of the eight lowest $^1\Sigma^+$ states of NH^{4+}.

Asymptote	Calculation	Experiment
$N^{3+}(2s^2;{}^1S)+H^+$	−63.962	−63.855
$N^{3+}(2s2p;{}^1P)+H^+$	−47.312	−47.651
$N^{3+}(2p^2;{}^1D)+H^+$	−40.027	−40.436
$N^{3+}(2p^2;{}^1S)+H^+$	−33.826	−34.673
$N^{3+}(2s3s;{}^1S)+H^+$	−15.506	−15.642
$N^{3+}(2s3p;{}^1P)+H^+$	−13.759	−13.700
$N^{3+}(2s3d;{}^1D)+H^+$	−10.274	−10.646
$N^{4+}(2s)+H(1s)$	(0.0)	(0.0)

wide range of R so that the calculations are straightforward.

As a test of the central difference approximation to $\langle\Psi_i|\partial/\partial R|\Psi_j\rangle$ embodied in Eq. (7), calculations were carried out for the states of the NHe^{5+} system treated by Bacchus-Montabonel [7], who used an alternative method that is based on the perturbation of a multiconfiguration wave function selected by an iterative process. The two sets of calculations employed the same basis sets and were carried out at the same nuclear separations. Except in regions of avoided crossings not considered in the perturbation methods, the potential curves and the nuclear coupling matrix elements are in excellent agreement. The matrix elements of $\partial/\partial R$ computed for the NH^{4+} system using the SCVB wave functions are reported in Table IV.

TABLE IV. Matrix elements of $\partial/\partial R$ for NH^{4+}.

R (bohr)	A_{43}	A_{42}	A_{41}
4.00	−0.0845		
4.25	−0.1041		
4.50	−0.1297		
4.75	−0.1643		
5.00	−0.2106	−0.0195	
5.25	−0.2707	−0.0649	
5.50	−0.3389	−0.1690	
5.75	−0.3964	−0.2926	
6.00	−0.4158	−0.4183	
6.25	−0.3773	−0.4894	
6.50	−0.3191	−0.4906	−0.0125
6.75	−0.2630	−0.4131	−0.0457
7.00	−0.1932	−0.3105	−0.0396
7.25	−0.1473	−0.2286	−0.0963
7.50	−0.1256	−0.1635	−0.1582
7.75	−0.1097	−0.1286	−0.5055
8.00	−0.0895	−0.0959	−1.4072
8.10			−2.0018
8.15			−2.1027
8.20	−0.0839	−0.0669	−1.9783
8.25	−0.0805		−1.6992
8.30	−0.0813	−0.0566	−1.4187
8.50	−0.0699		−0.6761
8.75	−0.0702	−0.0393	−0.2818
9.00	−0.0617	−0.0269	−0.1484
9.50	−0.0510	−0.0204	−0.0484
10.00	−0.0438	−0.0187	−0.0215

III. SCATTERING FORMALISM

In a space-fixed coordinate system, the nonrelativistic Hamiltonian for the NH^{4+} system is

$$H(\mathbf{R}_1,\mathbf{R}_2,\mathbf{r})=-\frac{1}{2M_1}\nabla^2_{R_1}-\frac{1}{2M_2}\nabla^2_{R_2}-\tfrac{1}{2}\sum_{i=1}^{N}\nabla^2_{r_i'}+\sum_{i=1}^{N}V_1(|\mathbf{R}_1-\mathbf{r}_1'|)+V_2(|\mathbf{R}_2-\mathbf{r}_i'|)+V_N(|\mathbf{R}_1-\mathbf{R}_2|)+V_{ee}\ , \tag{9}$$

where $\mathbf{R}_1,\mathbf{R}_2$ are the coordinates of the nitrogen and hydrogen nuclei, respectively, and $\mathbf{r}_i'$ are the electronic coordinates. The summations are over all N electronic coordinates V_1 and V_2 are the electron-nuclear interaction terms for the nitrogen and hydrogen nuclei, respectively, V_N is the internuclear repulsion, and V_{ee} is the electron-electron repulsion term. It is convenient to introduce a new set of coordinates $\{\mathbf{R}_{\text{c.m.}},\mathbf{R},\mathbf{r}_i\}$ related to the space-fixed coordinates by

$$\begin{aligned}\mathbf{R}_{\text{c.m.}}&=\frac{M_1\mathbf{R}_1+M_2\mathbf{R}_2+\sum_{i=1}^{N}\mathbf{r}_i'}{M}\ ,\\ \mathbf{R}&=\mathbf{R}_2-\mathbf{R}_1\ ,\\ \mathbf{r}_i&=\mathbf{r}_i'-\eta\mathbf{R}_1-(1-\eta)\mathbf{R}_2\ ,\end{aligned} \tag{10}$$

where $M=M_1+M_2+\sum_{i=1}^{N}$, and η is a parameter that determines the choice of origin for the electronic coordinates along the internuclear axis. Inserting Eq. (10) and

$$\begin{aligned}\nabla_{R_1}&=\frac{M_1}{M}\nabla_{R_{\text{c.m.}}}-\nabla_R-\sum_{i=1}\eta\nabla_{r_i}\ ,\\ \nabla_{R_2}&=\frac{M_2}{M}\nabla_{R_{\text{c.m.}}}+\nabla_R-\sum_{i=1}(1-\eta)\nabla_{r_i}\ ,\\ \nabla_{r_i'}&=\frac{1}{M}\nabla_{R_{\text{c.m.}}}+\nabla_{r_i}\ ,\end{aligned}$$

into Eq. (9), we get

$$H(\mathbf{R}_{\text{c.m.}},\mathbf{R},\mathbf{r}_i)=H_{\text{c.m.}}+H_{\text{KE}}(\eta)+V_N(\eta)+V_{ee}\ , \tag{11}$$

where $H_{\text{c.m.}}$ is the kinetic-energy operator for the center-of-mass motion and

$$H_{\text{KE}}(\eta)=-\frac{1}{2M_1}\left[\nabla_R+\eta\sum_{i=1}\nabla_{r_i}\right]^2-\frac{1}{2M_2}\left[\nabla_R-(1-\eta)\sum_{i}\nabla_{r_i}\right]^2-\tfrac{1}{2}\sum_{i=1}^{N}\nabla^2_{r_i}\ , \tag{12}$$

$$V_N(\eta)=\sum_{i=1}^{N}[V_1(|\mathbf{R}(1-\eta)+\mathbf{r}_i|)+V_2(|\eta\mathbf{R}-\mathbf{r}_i|)]+V_N(|\mathbf{R}|)\ , \tag{13}$$

are the kinetic energy and electrostatic interaction Hamiltonians, respectively. For the particular value $\eta=\eta_0=M_1/(M_1+M_2)$, the origin of the electron coor-

dinates is located at the center of mass of the two nuclei. For this choice of the origin, the kinetic-energy cross terms in Eq. (12) vanish. It is useful to express $H_{\rm KE}(\eta)$ for arbitrary η in terms of $H_{\rm KE}(\eta=\eta_0)$. We get

$$H_{\rm KE}(\eta)=U^{\dagger}H_{\rm KE}(\eta_0)U$$
$$=U^{\dagger}\left[-\frac{1}{2\mu}\nabla_R^2\right]U-\frac{1}{2(M_1+M_2)}\left[\sum_{i=1}\nabla_{r_i}\right]^2$$
$$-\tfrac{1}{2}\sum_{i=1}^{N}\nabla_{r_i}^2 , \tag{14}$$

where

$$U=\exp(\eta'\sum_{i=1}\nabla_{r_i}\cdot\mathbf{R})$$

is a translation operator, $\mu=M_1M_2/(M_1+M_2)$ is the reduced mass of the nuclei, and $\eta'=\eta-\eta_0$. In deriving Eq. (14) we made use of

$$U^{\dagger}\nabla_R U=\nabla_R+\sum_{i=1}\eta'\nabla_{r_i},\quad [\nabla_{r_i},U]=0 . \tag{15}$$

In the same manner, we get

$$V_N(\eta)=U^{\dagger}V_N(\eta_0)U . \tag{16}$$

We factor out the center-of-mass motion, and seek eigenfunctions of the Hamiltonian

$$H(\eta)=U^{\dagger}\left[-\frac{1}{2\mu}\nabla_R^2\right]U+H_{\rm ad}(\eta) , \tag{17}$$

where

$$H_{\rm ad}(\eta)=-\tfrac{1}{2}\sum_{i=1}\nabla_{r_i}^2-\frac{1}{2(M_1+M_2)}\left[\sum_{i=1}\nabla_{r_i}\right]^2+V_N(\eta)$$
$$+V_{ee} \tag{18}$$

is the adiabatic Hamiltonian. We use the quantal perturbed-stationary-state (PSS) approximation

$$\Psi(\mathbf{R},\mathbf{r}_i(\eta))=\sum_{\gamma}F_{\gamma}(\mathbf{R})\phi_{\gamma}(\mathbf{R},\mathbf{r}_i(\eta)) , \tag{19}$$

where the ϕ_{γ} are orthogonal eigenstates of the adiabatic Hamiltonian

$$H_{\rm ad}(\eta)\phi_{\gamma}=\varepsilon_{\gamma}(R)\phi_{\gamma} \tag{20}$$

to find the scattering solutions. In it, the sum over γ is restricted to a subset of the complete adiabatic set $\{\phi_{\gamma}\}$. We also refer to these states as channel states since each ϕ_{γ} correlates to an approximate atomic state in the asymptotic region.

The adiabatic eigenstates defined in Eq. (20) describe asymptotic states where the electron is coupled to the motion of the nuclei. They do not correlate to true atomic asymptotic states in which the electrons are coupled to the motion of the center of mass of the individual atoms. Electron translation factors [8] are often introduced to address this problem. However, for low-energy collisions of the type considered here, ansatz (19) is a valid approximation. We formulate below the PSS theory so that the invariance of the resulting scattering wave equation with respect to origin translation is explicitly demonstrated.

The eigenvalue $\varepsilon_{\gamma}(R)$ is the Born-Oppenheimer potential for the state γ and the eigenstates ϕ_{γ} are parametrized by the orientation of the internuclear axis, the origin parameter η, and internuclear distance. The PSS equations may be obtained by requiring that

$$\delta[\langle\Psi|H(\eta)|\Psi\rangle-E\langle\Psi|\Psi\rangle]=0 , \tag{21}$$

where δ is an arbitrary variation of the set $\{F_{\gamma}(\mathbf{R})\}$ and E is the collision energy, the bracket notation signifying integration over all coordinates. We express the adiabatic eigenstates for arbitrary η in terms of the adiabatic states defined for $\eta=\eta_0$ (nuclear center of mass):

$$\phi_{\gamma}(\mathbf{R},\mathbf{r}_i(\eta))=U^{\dagger}\phi_{\gamma}(\mathbf{R},\mathbf{r}_i(\eta_0)) , \tag{22}$$

where we have used Eqs. (15), (16), and (18). Using Eq. (22) in Eq. (19), expression (21) becomes

$$\delta\left[\int d^3R\,\{\underline{F}^{\dagger}[\nabla_R-i\underline{\mathbf{A}}(\mathbf{R})]^2\underline{F}-2\mu\underline{F}^{\dagger}[\underline{V}(\mathbf{R})-E]\underline{F}\}\right]$$
$$=0 , \tag{23}$$

where $\underline{F}^{\dagger}$ and $\underline{F}$ are row and column matrices, respectively, and the γth entry to $\underline{F}$ is the wave function $F_{\gamma}(\mathbf{R})$. The square matrices $\underline{\mathbf{A}}$ and $\underline{V}$ are defined below. Carrying out the variation we obtain the set of coupled equations [9]

$$\frac{-1}{2\mu}(\underline{I}\nabla-i\underline{\mathbf{A}})^2\underline{F}(\mathbf{R})+\underline{V}(\mathbf{R})\underline{F}(\mathbf{R})=E\underline{F}(\mathbf{R}) , \tag{24}$$

where

$$[\underline{\mathbf{A}}(\mathbf{R})]_{ij}=i\int d^3\mathbf{r}_1\cdots d^3\mathbf{r}_N\phi_i^*(\mathbf{R},\mathbf{r}_m(\eta))U^{\dagger}\nabla_R$$
$$\times U\phi_j(\mathbf{R},\mathbf{r}_m(\eta))$$
$$=i\int d^3\mathbf{r}_1\cdots d^3\mathbf{r}_N\phi_i^*(\mathbf{R},\mathbf{r}_m(\eta_0))$$
$$\times\nabla_R\phi_j(\mathbf{R},\mathbf{r}_m(\eta_0)) ,$$
$$[\underline{V}(\mathbf{R})]_{ij}=\delta_{ij}\varepsilon_i(R)+\sum_{\substack{k\neq i\\ k\neq j}}\frac{\mathbf{A}_{ik}\cdot\mathbf{A}_{kj}}{2\mu} \tag{25}$$

are vector and scalar potentials, and $\underline{I}$ is the unit matrix. The potentials given in (25) are independent of η' and the Schrödinger equation (24) and the S matrix, and do not depend on the choice of electronic coordinate origin along the internuclear axis.

We may solve Eq. (24) for $\underline{F}(\mathbf{R})$; but it is more convenient to introduce a new amplitude $\underline{G}=\underline{W}\,\underline{F}$, where $\underline{W}$ is a unitary matrix. If $\underline{F}$ is a solution to Eq. (24), then $\underline{G}$ is also a solution with the vector and scalar potentials $\underline{\mathbf{A}}$ and $\underline{V}$ replaced by

$$\underline{\mathbf{A}}'=\underline{W}\,\underline{\mathbf{A}}\,\underline{W}^{-1}+i\underline{W}\nabla_R\underline{W}^{-1} ,$$
$$\underline{V}'=\underline{W}\,\underline{V}\,\underline{W}^{-1} . \tag{26}$$

If the field strength tensor [9] associated with $\underline{\mathbf{A}}$ vanishes at all $\mathbf{R}$, then a transformation matrix $\underline{W}$ can be found so that the vector potential $\underline{\mathbf{A}}'$ also vanishes for all $\mathbf{R}$. This is the case for which $\underline{\mathbf{A}}$ does not possess angular com-

ponents, and is a function $\underline{\mathbf{A}}(R)=\hat{\mathbf{R}}\underline{A}(R)$ of the internuclear distance only. For it, we construct $\underline{W}$ by solving

$$\frac{d\underline{W}}{dR}+\underline{A}_R\underline{W}=0 \tag{27}$$

with the boundary condition $\lim R\to\infty \underline{W}_{ij}\to\delta_{ij}\varepsilon_i$. Using Eqs. (27) and (26), we obtain

$$\frac{-1}{2\mu}\underline{I}\nabla_R^2\underline{G}(\mathbf{R})+\underline{V}'(\mathbf{R})\underline{G}(\mathbf{R})=E\underline{G}(\mathbf{R}) , \tag{28}$$

in which $\underline{V}'$ is the diabatic potential [10] and its off-diagonal matrix elements are responsible for driving collision-induced atomic transitions. We solve for $\underline{G}$ by introducing a partial-wave decomposition

$$G_\gamma(\mathbf{R})=\sum_{l,m}\frac{g_\gamma^{lm}(R)}{R}Y_{lm}(\hat{R}) , \tag{29}$$

where Y_{lm} are the spherical harmonics. Inserting Eq. (29) into Eq. (28), we get the radial coupled equations

$$\left[\frac{d^2}{dR^2}-\frac{l(l+1)}{2\mu R^2}\right]g_\gamma^{lm}-2\mu\sum_{\gamma'}U_{\gamma,\gamma'}(R)g_{\gamma'}^{lm}+2\mu E g_\gamma^{lm}=0 , \tag{30}$$

$$U_{\gamma,\gamma'}(R)\equiv[\underline{W}\,\underline{V}\,\underline{W}^{-1}]_{\gamma\gamma'} .$$

The radial functions satisfy the scattering boundary conditions

$$\lim_{R\to\infty}g_\gamma^{lm}(R)\to\frac{1}{\sqrt{k_{\gamma'}}}\left[\delta_{\gamma,\gamma'}j_l(k_\gamma R)+K^l_{\gamma,\gamma'}\eta_l(k_{\gamma'}R)\right] , \tag{31}$$

$$k_\gamma=\sqrt{2\mu[E-\varepsilon_{\gamma\gamma}(\infty)]} ,$$

where j_l, and η_l are, respectively, the regular and irregular Bessel-Ricatti functions [11] for neutral channels, and the regular and irregular Coulomb functions [11] for the Coulomb channels. $K^l_{\gamma,\gamma'}\equiv\underline{K}^l$ is a real symmetric matrix and the S matrix is given by

$$\underline{S}^l=\frac{\underline{I}+i\underline{K}^l}{\underline{I}-i\underline{K}^l} . \tag{32}$$

The cross section for the system to undergo an inelastic transition from atomic state i to j is

$$\sigma(i\to j)=\frac{\pi}{k_i^2}\sum_l(2l+1)|\underline{S}^l|^2_{i,j} . \tag{33}$$

IV. RESULTS AND DISCUSSION

The Born-Oppenheimer potentials for the exothermic channels of $^1\Sigma$ symmetry separating to N^{+3} and H, which lie below doubly excited $2p3l$ states and the singly excited $2s4l$ states, are illustrated in Fig. 1 and listed in Table II. Capture into the states separating to $N^{3+}(2p3l)$ involves a two-electron transition. The interaction with the entrance channel is correspondingly weak and capture leading to the doubly excited ions makes only a small contribution to the total charge-transfer cross sections. Capture into the states separating to $N^{3+}(2s4l)$ involves a one-electron transition, but the avoided crossings occur at large internuclear distances around $75a_0$ and the capture probability is negligible. Because we are primarily interested in the cross sections for charge transfer at low collision energies, we restrict the expansion basis in the scattering equations to the $^1\Sigma^+$ states that have the separated-atom limits $N^{4+}(2s)+H$, $N^{3+}(2s3d)+H^+$, $N^{3+}(2s3p)+H^+$, and $N^{3+}(2s3s)+H^+$. The remainder of the adiabatic states whose potential curves are shown in Fig. 1 but are not included in expansion (19) contribute at collision energies higher than the ones of interest here. States with Π symmetry are not included in (19) since the radial adiabatic coupling between Σ states is the predominant charge-transfer mechanism at lower collision energies. We set the label $\gamma=4$ for the neutral $N^{4+}+H$ channel, and $\gamma=3,2,1$ for the Coulomb channels $N^{3+}(3d)+H^+$, $N^{3+}(3p)+H^+$, and $N^{3+}(3s)+H^+$, respectively.

In the adiabatic picture the scattering equations are given by Eq. (23). In this picture, the charge-transfer transitions are driven by the off-diagonal elements of the vector potential matrix $\underline{\mathbf{A}}$. The higher-order term proportional to $1/2\mu$ in the scalar potential matrix $\underline{V}$ is small and is neglected. Because we are dealing with adiabatic states of Σ symmetry, the adiabatic vector coupling matrix has nonvanishing radial components that are functions of the internuclear distance only, i.e., $\underline{\mathbf{A}}=\hat{\mathbf{R}}\underline{A}(R)$. In Fig. 2 we plot the matrix coupling elements $A_{43}(R)$, $A_{42}(R)$, and $A_{41}(R)$, where the subscripts refer to the

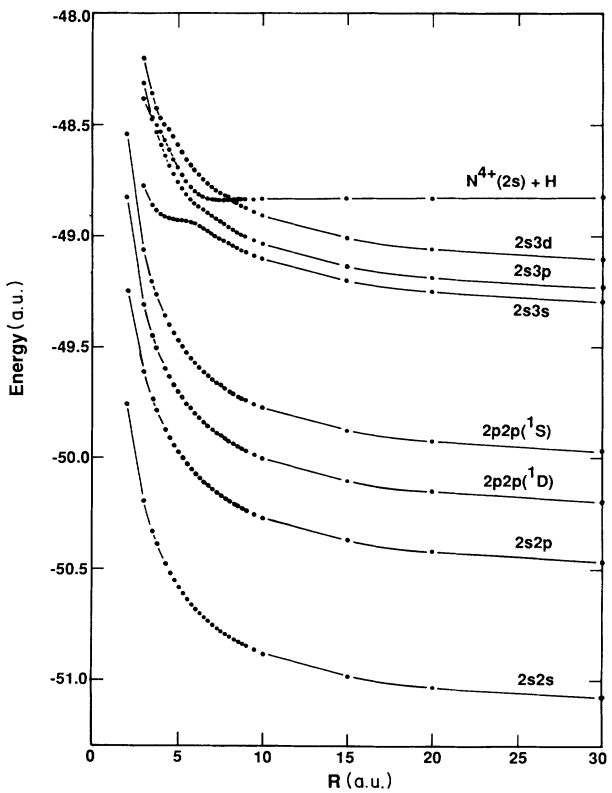

FIG. 1. Adiabatic $^1\Sigma^+$ potential curves for the NH^{4+} system as function of the internuclear distance R. The states are labeled by $nln'l'$, the electronic configuration of the N^{3+} ion.

channel indices and

$$A_{ij}(R)=\left\langle \phi_i \left| \frac{\partial}{\partial R} \right| \phi_j \right\rangle , \tag{34}$$

where the angle brackets signify integration over all electronic coordinates. In Fig. 2, $A_{43}(R)$ is the dominant matrix element. It has a narrow Gaussian profile centered at $R \approx 8.1$ bohr, a region near a strong avoided crossing (see Fig. 1) of the adiabatic potential-energy curves for the $N^{3+}(3d)+H^+$ and $N^{4+}+H$ states. The $A_{42}(R)$ and $A_{41}(R)$ functions have similar but broader and shallower Gaussian shapes centered at $R \approx 6.2$ and 6.0 bohr, respectively. The peaks correspond to weak avoided crossings (not discernible in Fig. 1) between the $N^{4+}+H$ and the $N^{3+}(2s3p)+H^+$, $N^{3+}(2s3s)+H^+$ adiabatic potential curves. The couplings A_{32}, A_{31}, and A_{21} do not contribute to the direct charge-transfer process in first order and so we do not include them in our approximation. We use the fact that $\underline{\mathbf{A}}$ is a Hermitian matrix to find the remaining matrix elements.

It is possible to solve the adiabatic equations (24) for the S matrix, but it is more convenient to work in the diabatic picture. In this picture the scattering equations are given by Eq. (28), and the charge-transfer transitions are driven by the off-diagonal matrix elements of the diabatic potential $\underline{V}'$. We calculated the diabatic potential matrix by first solving Eq. (27) for the transformation matrix $\underline{W}$,

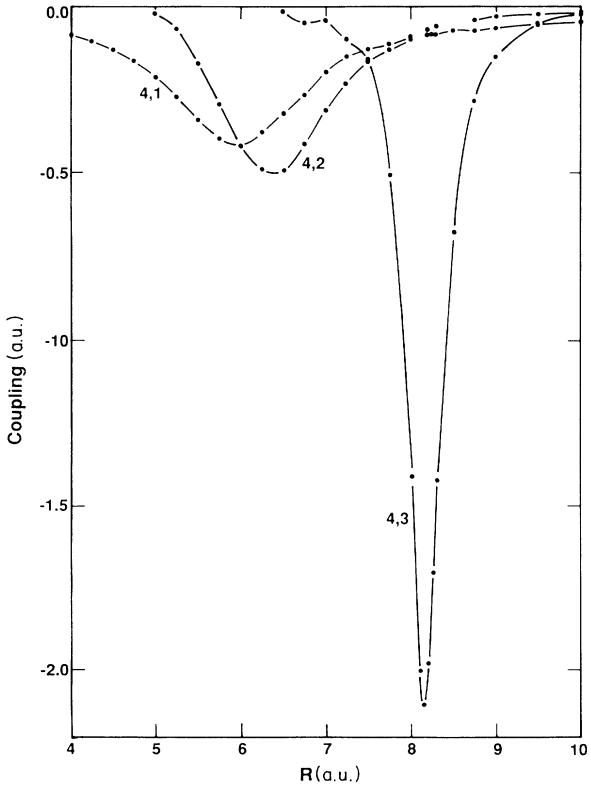

FIG. 2. Radial adiabatic matrix elements $A_{ij}(R)$ as a function of the internuclear distance R. The subscripts refer to the channels assignment given in the text.

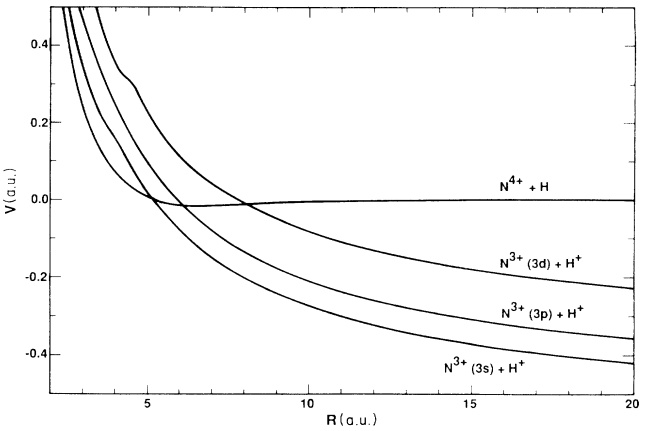

FIG. 3. Diabatic $^1\Sigma^+$ potentials for the NH^{4+} system as a function of the internuclear distance R. The labels correspond to the asymptotic atomic limits of the diabatic potentials.

and then using the transformation law (26). The diagonal elements of the diabatic potential matrix are illustrated in Fig. 3. In the molecular region the diabatic and adiabatic curves differ significantly. The avoided crossings in the adiabatic picture are real crossings in the diabatic picture. In the asymptotic region, at large R the adiabatic and diabatic potential curves are identical and approach the asymptotic atomic energies. The off-diagonal elements of the diabatic potential matrix are shown in Fig. 4. Unlike the adiabatic coupling matrix elements, the diabatic couplings are not localized and do not display a Gaussian profile. Instead, they exhibit broad features throughout the molecular region. We reduce the diabatic Schrödinger equation (28) to a set of radial equations (30), which we solve using an implementation of the logarithm-derivative method of Johnson [12].

The cross sections for the three state-selective charge-transfer transitions are illustrated in Fig. 5. At low collision energies the $N^{4+}+H \rightarrow N^{3+}(3d)+H^+$ charge-transfer cross section $[\sigma(4\rightarrow 3)]$ is predominant, and in the collision-energy range between 0.1 and 10 eV, the cross sections for charge transfer into the $3p$ and $3s$ states

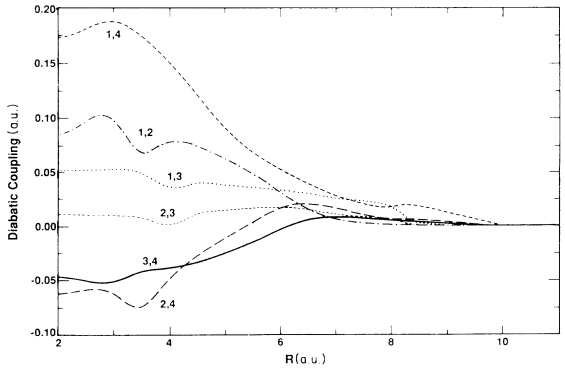

FIG. 4. Diabatic off-diagonal coupling curves for the NH^{4+} system as a function of the internuclear distance R. Subscripts refer to the channel index given in the text.

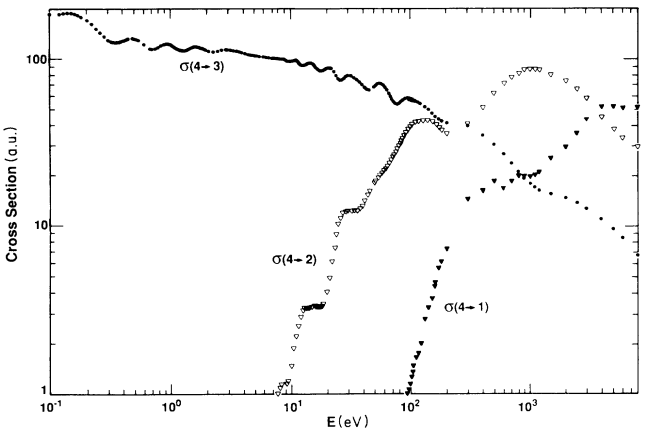

FIG. 5. State-dependent charge-transfer cross sections $\sigma(i \rightarrow j)$, where i,j, represent the initial and final channel index, respectively, given in the text. E is the collision energy in the center-of-mass frame in units of eV.

of N^{3+} are negligible. At 0.1 eV, $\sigma(4 \rightarrow 3)$ has the value 5.2×10^{-15} cm^2, and as the collision energy increases, $\sigma(4 \rightarrow 3)$ decreases. In the entire energy range the cross sections exhibit strong oscillatory behavior superimposed on a general monotonic trend. We interpret these structures as a type of Stueckelberg oscillation [13].

Wave phenomena such as rainbow scattering, and glory and Stuekelberg oscillations have been observed in the measurements of the elastic and inelastic differential cross sections for charge transfer in various systems [14]. Stuekelberg oscillations are associated with the rapid variation of the differential cross section with respect to the scattering angle. When the differential cross section is angle integrated, the averaging effect usually results in a total cross section that varies smoothly with collision energy. However, oscillations in the total charge-transfer cross sections with respect to the collision energy have been observed in inelastic asymmetric ion-atom collisions at high energies [15].

Within the two-state approximation the cross section for charge transfer from channel 0 to 1 may be expressed by the general formula [16]

$$Q_{0\rightarrow 1} = \frac{4\pi k_1}{k_0} \sum_l \frac{(2l+1)\chi_l^2}{(k_0 + k_1 \chi_l^2)^2} \sin^2(\tau_l), \quad \tau_l \equiv \delta_l^a - \delta_l^b \ , \tag{35}$$

where k_0, and k_1 are the wave numbers for the entrance and exit channels, respectively, χ_l is the mixing parameter [16], and δ_l^a, and δ_l^b are coupled-channel phase shifts [16]. Olson [13] used an analytic stationary-phase procedure and a semiclassical approximation for the phase shifts. He showed that Stuekelberg oscillations persist in the angle-averaged total cross sections, and identified these features in the experimental measurements of Perel, Vernon, and Daley [15].

We have used the semiclassical approximation for the phase shift τ_l in a two-state approximation to $\sigma(4 \rightarrow 3)$ shown in Fig. 5. Because we are concerned here with low-energy collisions, the high-energy analytic approximation of Olson is not valid here. We evaluated all semiclassical phase shifts numerically and were able to reproduce all the local peaks in $\sigma(4 \rightarrow 3)$ illustrated Fig. 5. We conclude that the structures in $\sigma(4 \rightarrow 3)$ are a manifestation of the Stueckelberg oscillations. Although we have been successful in reproducing the oscillatory structure within the semiclassical approximation, the absolute values of the cross section are not predicted accurately in this approximation. A complete detailed description of the semiclassical calculation will be presented elsewhere.

At collision energies near 200 eV, $\sigma(4 \rightarrow 2)$ increases rapidly and is equal to $\sigma(4 \rightarrow 3)$ at 290 eV, with a value of 1.1×10^{-15} cm^2. At energies between 0.2 and 2 keV, charge transfer into the $N^{3+}(3p)$ state dominates.

The qualitative features of these cross sections may be understood from the diabatic potential curves shown in Fig. 3. We view charge transfer occurring because the $N^{4+}+H$ potential curve, in which the ion and the hydrogen atom initially approach, crosses the potential curve of a molecular state that correlates to one of the $N^{3+}+H^+$ atomic states. During the approach, the system makes a transition at the crossing and exits into one of the $N^{3+}+H^+$ repulsive Coulomb curves. In Fig. 3 the first crossing occurs near $R=8$ bohr, where the potential $N^{4+}+H$ curve crosses the $N^{3+}(3d)+H^+$ curve. At low collision energies the approaching nitrogen ion and hydrogen atom do not have enough energy at the larger impact parameters to penetrate the small R region. Therefore, states whose potential curves cross at larger internuclear distances are more accessible to the colliding systems and charge transfer into them is favored. This argument explains the large cross section, at low energies, into the $N^{3+}(3d)$ state. At higher collision energies the colliding system samples the regions with smaller R, and charge transfer into states with crossings at smaller R become significant. This simplified picture is consistent with the detailed quantum-mechanical calculations of the cross sections illustrated in Fig. 5.

We have carried out calculations only for the singlet states of the quasimolecule. We expect that at intermediate energies the singlet and triplet cross sections are not sensitive to small differences in the singlet and triplet molecular curves. In Fig. 6 we present the sum of the charge-transfer cross sections into the $N^{3+}(2s3l)$ states and compare them to the total charge-transfer cross sections measured by Huq, Havener, and Phaneuf [2]. The agreement is close between energies of 4.1 and 182 eV/amu. The close agreement suggests that the singlet and triplet cross sections are indeed similar and that capture into $N^{3+}(2s3l)$ is the dominant charge-transfer mechanism. The total cross section has a local maximum at 70 eV/amu. At 70 eV/amu the cross sections for capture into $N^{3+}(3d)$ and $N^{3+}(3p)$ are similar, with values of 1.4×10^{-15} and 8.44×10^{-16} cm^2, respectively.

At velocities below 4.1 eV/amu differences occur between the measured and total singlet cross sections. Some of the discrepancy is due to the greater sensitivity of the predictions to the molecular parameters at low energies and the failure of our assumption that the singlet and triplet cross sections are comparable. However, we

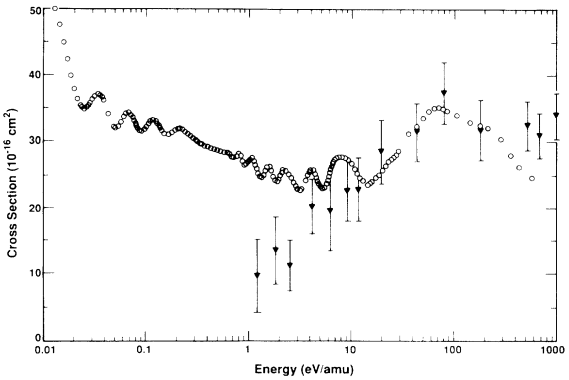

FIG. 6. Total calculated singlet-state charge-transfer cross section $N^{4+}+H \rightarrow \sum_{l=s,p,d} N^{3+}(3l)+H^+$ (open circles). Total measured cross section for process $N^{4+}+H \rightarrow N^{3+}+H^+$ from Ref. [2] (filled triangles). E is the collision energy.

do not believe all of the discrepancy can be attributed to defects in the theoretical approach at low energies. The theory makes the strong prediction that the cross section will ultimately rise rapidly at low energies as the long-range polarization attraction causes trajectories to pass through the crossing region. In contrast the measured cross section appears to be diminishing toward low energies. At energies above 500 eV/amu, additional channels begin to play a major role and our theoretical predictions become uncertain.

In Table V we present the calculated rate coefficient corresponding to a Maxwellian distribution for the process (1) in the range of gas temperatures from 10^4 to 10^7 K. We compare our calculated rates to those given in Ref. [2]. At low temperatures the two rates are comparable. At these energies, charge transfer into the $N^{3+}(3d)$ state is the dominant one and our cross sections are in rough agreement with the ones obtained by Huq, Havener, and Phaneuf. At higher temperatures the rate coefficients given here are significantly larger than those reported in Ref. [2]. The behavior of the state-dependent cross sections as a function of the collision energy differ for the two calculations. In our calculation the cross section for charge transfer into the $N^{3+}(3p)$ state becomes comparable with the cross section into the $N^{3+}(3d)$ state at around 200 eV, whereas in Ref. [2], this occurs at a much lower energy (around 20 eV).

TABLE V. Calculated rate coefficients for the singlet charge-transfer process (1). The rate coefficients are given in units of 10^{-9} cm^3/s.

T (K)	Rate	Rate (from Ref. [2])
1×10^4	5.4	3.8
3×10^4	8.5	5.4
1×10^5	14	8.2
3×10^5	22	
6×10^5	32	
1×10^6	42	
3×10^6	83	
1×10^7	170	

The $N^{3+}(3d)$ state radiates preferentially to the $N^{3+}(2p)$ state, giving rise to emission lines near 28.35 nm but there is a weak transition to the $N^{3+}(3p)$ state with a branching ratio of 2×10^{-3} at a wavelength of 405.8 nm.

ACKNOWLEDGMENTS

B. Zygelman and A. Dalgarno are supported by the U.S. Department of Energy Office of Basic Energy Sciences, Division of Chemical Sciences. We thank the National Energy Research Supercomputer Center (NERSC), at which the collision calculations were performed. B. Zygelman also thanks the National Supercomputer Center for the Environment and Energy (NSCEE) at the University of Nevada, Las Vegas, for the use of their supercomputer. We thank M. S. Child for bringing to our attention Ref. [13].

[1] C. A. Feickert, R. J. Blint, G. T. Surrat, and W. D. Watson, Astrophys. J. **286**, 371 (1984).
[2] M. S. Huq, C. C. Havener, and R. A. Phaneuf, Phys. Rev. A **40**, 1811 (1989).
[3] D. L. Cooper, M. J. Ford, J. Gerratt, and M. Raimondi, Phys. Rev. A **34**, 1752 (1986); S. A. Barnard, M. J. Ford, D. L. Cooper, J. Gerratt, and M. Raimondi, Mol. Phys. **61**, 1193 (1987).
[4] D. L. Cooper, J. Gerratt, M. Raimondi, and M. Sironi, J. Chem. Phys. **87**, 1666 (1987).
[5] D. L. Cooper, J. Gerratt, and M. Raimondi, Adv. Chem. Phys. **69**, 319 (1987); Int. Rev. Phys. Chem. **7**, 59 (1988); in *Valence Bond Theory and Chemical Structure,* edited by D. J. Klein and N. Trinajstic (Elsevier, Amsterdam, 1990).
[6] D. L. Cooper, J. Gerratt, and M. Raimondi, Chem. Rev. **91**, 929 (1991).
[7] M. C. Bacchus (private communication); M. C. Bacchus-Montabonel, Phys. Rev. A **36**, 1994 (1987).
[8] D. R. Bates and R. W. McCarroll, Proc. R. Soc. London Ser. A **245**, 175 (1958).
[9] B. Zygelman, Phys. Lett. A **125**, 476 (1987); Phys. Rev. Lett. **64**, 256 (1990).
[10] F. T. Smith, Phys. Rev. **179**, 111 (1969); T. G. Heil, S. Butler, and A. Dalgarno, Phys. Rev. A **23**, 1100 (1981).
[11] *Handbook of Mathematical Functions,* edited by M. Abramowitz and I. A. Stegun (Dover, New York, 1970).
[12] B. R. Johnson, J. Comput. Phys. **13**, 445 (1973).
[13] R. E. Olson, Phys. Rev. A **2**, 121 (1970).
[14] L. R. Andersson, J. O. P. Pederson, A. Barany, J. P. Bangsgaard, and P. Hvelpund, J. Phys. B **22**, 1603 (1989); G. L. Lockwood, H. F. Helbig, and E. Everhart, Phys. Rev. **132**, 2078 (1965).
[15] J. Perel, R. H. Vernon, and H. L. Daley, Phys. Rev. **138**, A937 (1965).
[16] M. F. Mott and H. S. W. Massey, *The Theory of Atomic Collisions* (Clarendon, Oxford, 1965), Chap. XIII.